


RESEARCH ARTICLE

Torque, speed, and power requirements for the design of a lower limb exoskeleton to augment human finned swimming

Beau Johnson  and Michael Goldfarb

Mechanical Engineering, Vanderbilt University, Nashville, TN, USA

Corresponding author: Beau Johnson; Email: beau.p.johnson@vanderbilt.edu

Received: 28 November 2023; **Revised:** 21 May 2024; **Accepted:** 6 August 2024

Keywords: design; exoskeletons; human biomechanics; mechatronic systems; robot dynamics

Abstract

The authors seek to design a lower limb exoskeleton to augment human finned swimming; however, data associated with human finned swimming previously did not exist, particularly data that characterizes the active joint torque requirements for human-scale finned swimming motion and the corresponding thrust generation. Since these data are not directly measurable nor easily computed in human subject experiments, the authors instead employed a human-scale robotic platform to characterize the relationship between joint torque, speed, power, and thrust production during flutter kick swimming, specifically at the hip joints. Among the useful insights from this study: (1) the underwater environment can be accurately modeled as a simple viscous load as seen by the hip joints, where viscous coefficient depends on the type of fin; (2) accordingly, for a given fin, movement at any amplitude and frequency is invariant when motion is normalized by amplitude; velocity and torque by the product of amplitude and frequency; and power and thrust by the square of the product of amplitude and frequency; (3) the power-specific thrust is invariant, regardless of fin type, amplitude of motion, and frequency of motion; and 4) the phasing between right and left legs does not have a significant effect on thrust generation (i.e., kicking in-phase and kicking in opposition behave similarly). The authors hope this data will be useful to other researchers interested in developing lower limb exoskeletons to augment underwater human finned swimming.

1. Introduction

Although several lower limb exoskeletons have been developed to augment human-legged locomotion [1], few have been developed to augment human swimming. Development of exoskeletons for legged locomotion has been greatly facilitated by biomechanical studies that have characterized the movement kinematics and kinetics (i.e., joint torque, speed, and power requirements) associated with walking, running, and other legged activities (e.g., [2, 3]). These data were obtained via camera-based motion-capture systems used in conjunction with force plates and model-based inverse dynamics computations.

Little if any similar data exist for human finned swimming. Among the reasons, underwater motion capture is more challenging than overground, and obtaining kinetic data associated with underwater movement is particularly challenging. In the case of walking or running, external forces are relatively easily measured at singular points of contact (i.e., between each foot and the ground) via force plates, and dynamic models entail well-known inertial and gravitational forces. In the case of swimming, environmental forces (i.e., between the water and human) are highly distributed and not easily measurable. Further, even if these forces were measured, analytical models of the dynamics of a human interacting with a fluid in which they are immersed are not easily employed to compute joint torque and power via inverse dynamics, as is common in overground biomechanics. As such, data characterizing human finned swimming biomechanics, and joint torque and power in particular, are not readily available.

Literature on swimming robotics could potentially inform the requirements for a finned swimming exoskeleton, although the engineering literature on swimming robots has primarily focused on mimicking the motions of non-human swimmers, such as fish [4], eels [5], and other aquatic animals [6, 7]. Evaluations of two humanoid robots have been conducted and reported propulsive measurements, but one platform does not utilize fins [8], and the other is not human-scale [9]. Thus, the development of swimming robots has contributed relatively little to the understanding of finned human swimming and associated movement kinematics and kinetics.

Although some efforts have been made towards swimming exoskeletons [10–12], and studies exist characterizing swimming motion of human flutter kicking and finned swimming [13–15], these studies do not describe joint torque or power requirements. Specifically, no prior work has been published characterizing the kinetics of a bilateral finned flutter kick – namely, the input torque and power associated with a given amount of thrust generation. This information is particularly important for the design and development of a lower limb exoskeleton for augmentation and/or assistance of human finned swimming.

Previously, the authors reported on a robotic testbed with offboard actuation, wherein the hip joints were driven via Bowden cables [16]. The setup, however, was heavily torque limited, and compliance in the transmission limited the ability to control movement. Further, that setup did not include sensing to measure joint torque output (torque was estimated from motor current and friction models of the transmission) or sensing to measure thrust (thrust was instead computed using camera-based measurement of fin motion combined with fluid mechanics models). Based on lessons learned from the initial experimental setup described in ref. [16], the authors developed a “second-generation” bilateral robotic finned swimming testbed, which unlike the previous version includes (1) onboard actuation that enables substantially greater torque and power generation (approximately 4x the capabilities of [16]), and also substantially improved joint-level control; (2) direct measurement of joint torque via custom onboard load cells at each hip joint; and 3) an onboard load cell setup that measures thrust directly. This testbed was used to conduct a series of experiments described herein to characterize the relationship between joint-space torque and power and the resultant thrust over a span of kick parameters (i.e., kick frequency and amplitude) commensurate with human-scale finned swimming [13–15].

Therefore, in order to provide the design requirements for a lower limb exoskeleton capable for augmenting human finned swimming, this paper describes the design of a “second-generation” testbed and then presents kinematic and kinetic data from a series of finned flutter-kicking experiments that characterize exoskeletal joint-space requirements for providing exoskeletal augmentation of finned swimming. These data form an essential foundation upon which researchers can design lower limb exoskeletons to augment finned swimming, specifically by providing detailed information with respect to joint torque, speed, and power requirements needed to provide a desired amount of underwater thrust.

2. Methods

2.1. Experimental apparatus

A robotic platform was constructed in order to conduct experiments to characterize the hip joint kinematics and kinetics associated with finned swimming and its associated thrust production. Biomechanical studies have clearly established that maximum efficiency in underwater finned swimming results when movement is “generated in the hip joint, with a small range of motion performed in the knee and ankle joints. The use of such kicking technique ensures that the fin blade moves perpendicularly to the water surface, generating a greater propulsive force” (e.g., [14, 17]). It should be noted that knee movement results in increased drag forces relative to propulsive forces, which lowers the net thrust across a full stroke. Thus, in order to maintain consistency with the preferred finning techniques for maximum propulsive efficiency, a lower limb exoskeleton should augment the hip joints actively (i.e., with powered joints) and augment the knee and ankle joints passively (i.e., with appropriate stiffness) to essentially hold both joints fully extended. Passive augmentation of the knee and ankle joints also enables an exoskeleton with fewer powered degrees of freedom and lower rotational inertia about the hip joints. Consistent

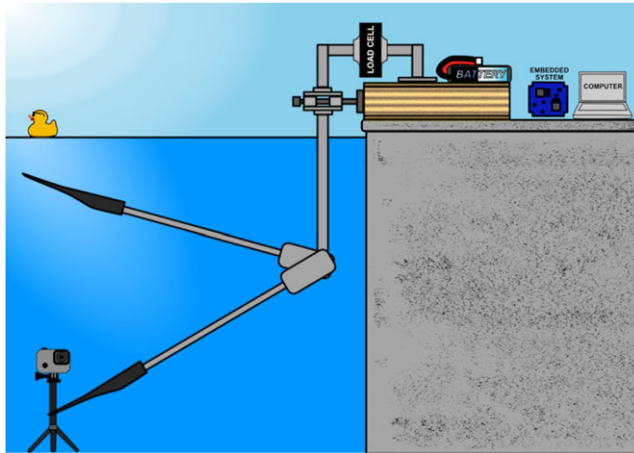


Figure 1. Illustration of the robotic flutter kicking platform.

with this approach, the experimental exoskeletal device described herein employs bilateral powered hip joints to power fin movement, in addition to bilateral passive knee and ankle joints to essentially maintain knee and ankle joints at or near full extension. The robotic apparatus further includes sensing of motion and torque at each hip joint, and also includes sensing for net thrust production generated by the robotic swimmer (as subsequently described); as such, hip motion, torque, and power could be measured directly, in addition to the resulting thrust production.

The experimental platform, illustrated in Figure 1, is comprised of a pair of hip joint actuation drive units, each of which drives a swim fin through a leg link approximately 1.0 m (39 in) in length (i.e., the approximately length of a human leg). The configuration of each hip joint actuation unit is shown in Figure 2; specifically, each drive unit is comprised of a frameless, brushless DC motor (Allied Motion MF0095020), which drives the respective hip joint through a three-stage 90:1 chain drive transmission, such that the unit (neglecting inefficiency) should be capable of providing 150 Nm of continuous torque at each joint. Each hip joint drive unit is sealed to prevent water ingress, such that it can be submerged without detriment to the motor, transmission, or internal electronics. Among the latter are Hall-based absolute angle sensors that measure the absolute angle at each hip joint (AMS model no. AS5145H), Hall-based incremental angle sensing at each motor, and hip joint torque sensing via a full strain gage bridge at the output of each hip joint (Micro-Measurements C4A-13-235SL-350-23P). During characterization experiments, the robotic swimmer was submerged and mounted to a platform anchored to the side of a pool by a plate supported on linear bearings. A load cell (Transducer Techniques MLP-75) was affixed between the sliding plate and ground platform, which measured the horizontal component of instantaneous thrust production generated by the robotic swimmer. The combination of sensors enables control of the kicking motion, measurement of torque and power at each hip joint, and measurement of the resulting thrust generation.

A custom embedded system was employed to drive the two brushless motors, measure from the sensors, and interface the sensors and actuators with a laptop computer for control and data collection. The brushless motor control was provided via a microprocessor optimized for signal processing (Microchip DSPIC 33FJ64GS608-E/PT), which communicates via SPI with a 32-bit general-purpose microcontroller (Microchip PIC32 MZ2048EFM100-I/PF), which communicates via a CAN bus with a laptop computer. The system was powered by three four-cell, 6.0 Ah lithium polymer batteries (Thunder Power RC 6000 mAh 4S 14.8V ProLite X 25C LiPo) wired in series to achieve a nominal supply voltage of 45 V. To prevent the need for waterproofing electrical components, the embedded system, computer, and batteries were housed above-ground, with electrical cables extending into the water and into the actuation units through sealed connections.

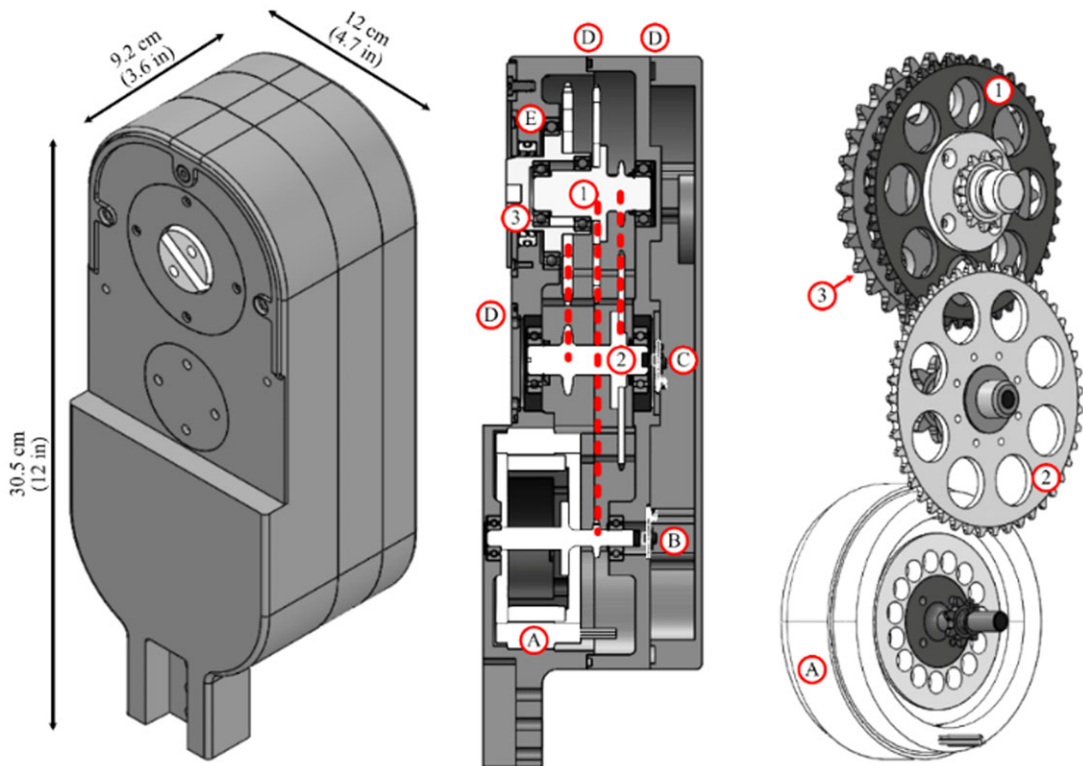


Figure 2. CAD model of the actuation unit highlighting: (1-3) the 3 stages of the transmission, (A) Frameless BLDC motor, (B) Incremental encoder, (C) Absolute encoder, (D) Static seals, and (E) Rotary output seal.

2.2. Control

A flutter kicking swimming motion consists essentially of two phases: (1) a power stroke/phase, characterized by flexion of the hip joint and downward movement of the fin; and (2) a recovery stroke/phase, characterized by extension of the hip joint and upward movement of the fin. The angle trajectory of each hip joint follows an essentially sinusoidal path, with the right and left legs approximately 180 deg out-of-phase with each other (i.e., when the right leg executes a power stroke, the left executes a recovery stroke). In order to characterize the effect of kick amplitude and frequency on thrust generation, the experiments described herein were conducted using trajectory control around each hip joint, which each was controlled to track a sinusoidal motion of prescribed amplitude and frequency, with each hip joint 180 deg out-of-phase with the contralateral hip joint. As described in the experimental trials section, additional trials were also conducted evaluating the thrust characteristics when the two hip joints were controlled to move in-phase, but otherwise with the same trajectory controller.

2.3. Swim fins

Two different models of fins were evaluated in this work: (1) a large, stiff fin (ScubaPro Jet Fins, Johnson Outdoors, Racine WI), representative of fins used by experienced divers; and (2) a short, flexible fin (Tyr Split Fins, Tyr Sport, Huntington Beach CA), representative of those used by recreational swimmers. Both types of fins increase the thrust production of a swimmer in comparison to swimming barefoot. Larger, stiffer fins are typically capable of greater thrust generation, but require greater torque and power to move through the water, thereby requiring greater strength and effort from the swimmer.

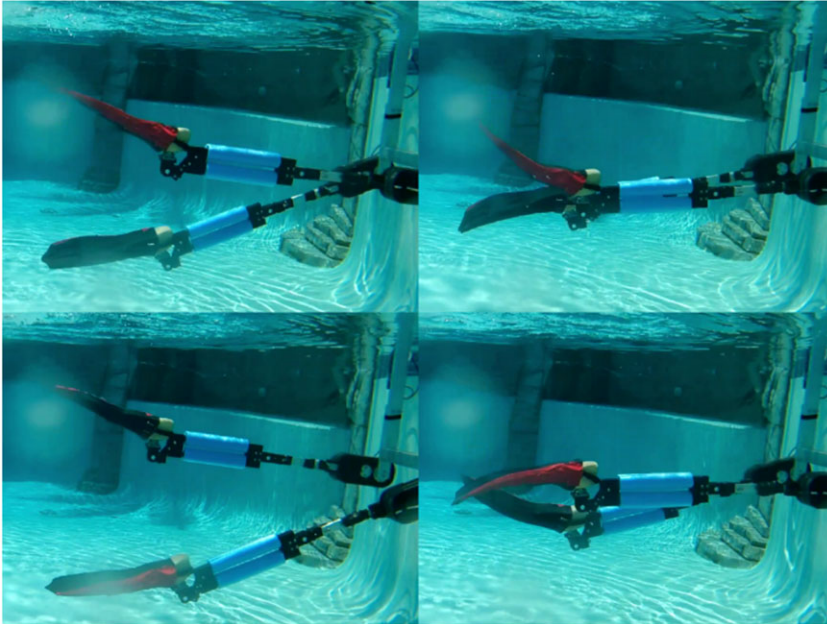


Figure 3. Frames from a video of an experimental trial. A corresponding video of experimental trials is included with the supplemental material submitted with this paper.

2.4. Experimental trials

The robotic platform was submerged under water in a swimming pool and affixed to a platform anchored on the side of the pool, as illustrated in Figure 1 and shown in video frames in Figure 3. As shown in Figure 3, short lengths of (blue) polyethylene foam (i.e., closed-cell foam) were affixed to each lower leg to provide approximate neutral buoyancy for each leg. Trials employed sinusoidal hip motion, where the motion amplitude and frequency were varied in each trial in order to span a space of movement characteristics. Four different desired hip motion amplitudes were used – 10, 20, 30, and 40 deg of hip motion. Note that amplitude in this paper refers to the peak-to-peak amplitude of the sinusoidal hip motion. At each hip amplitude and for each fin type (long and short), a highest experimental frequency was determined as one that saturated the robotic system at either a maximum torque, speed, and/or power. The frequencies used in each trial spanned frequencies between 0.25 Hz and the highest determined frequency for the given amplitude of motion and fin type. For the long fin, trials were conducted at five different frequencies for each amplitude; for the short fin, four different frequencies were tested. Note that, as one exception, the 20 deg amplitude series for the long fins only used four frequencies instead of five. Therefore, in total, 19 trials were conducted with the long, stiff fins across different movement amplitudes and frequencies of motion, and 16 trials were conducted with the short, flexible fins across different movement amplitudes and frequencies. Recorded data included hip joint motion, torque for each hip, and thrust generated by the platform, (all recorded in MATLAB), along with video recordings of each trial (video taken with a Crosstour Sports Action Camera). A video of representative experimental trials at various experimental conditions is included with the supplemental material submitted with this paper.

3. Results

3.1. Movement kinematics and kinetics of a finned flutter kick

The normalized mean and standard deviation of hip motion, torque, and power for all trials are shown in Figure 4. To be clear, the data shown in this figure represents approximately 1100 kicking strokes

across 35 different stroke conditions, all of which result in the plots shown in Figure 4 when normalized as described here. For each fin, movement amplitude, and movement frequency, data was collected over a 25 s period after the system achieved a steady-state motion (i.e., after startup transients). The data were segmented into strokes, where each segment start was aligned with the start of the power stroke (i.e., the zero crossing of hip velocity between the recovery and power strokes). Figure 4(a) therefore shows the measured hip angle as a function of stroke, normalized by the amplitude of the desired hip angle; Figure 4(b) shows the hip angular velocity as a function of stroke, differentiated from the angle measurement, normalized by the product of the desired hip angle amplitude and frequency (in Hz); Figure 4(c) shows the measured hip joint torque, also normalized by the product of the desired hip angle amplitude and frequency; Figure 4(d) shows the measured hip joint power, computed as the product of the normalized torque and velocity, (i.e., the product of the torque and velocity normalized by the square of the product of the desired hip angle amplitude and frequency); and Figure 4(e) shows the measured thrust production of the motion, also normalized by the square of the product of amplitude and frequency. Note that data shown in Fig 4(a-d) are plotted for an individual hip joint, but the thrust production (Figure 4(e)) shows the measured thrust when kicking with both legs. The solid lines show the mean of all data with the long fins, while the dashed lines show the means of all data with the short fins. The color band around each line indicates plus and minus one standard deviation of the data across all trials (for each respective fin type). The data associated with the solid lines therefore represents approximately 600 strokes (i.e., all long fin trials, both legs), while the data associated with the dashed lines represents approximately 500 strokes (i.e., all short fin trials, both legs). One should note that the vertical axis (i.e., the ordinate axis) on Figure 4(a) is inverted, such that negative numbers are shown above zero and positive numbers below. Although unconventional, this representation maintains the biomechanical convention of hip flexion as a positive angle, while also maintaining a visual correlation between the hip angle and vertical fin position (i.e., the fin is at its highest point when the hip angle is most negative). The authors believe this makes the data easier to understand.

Given the small variance around each line type in Figure 4, it is clear that data corresponding to a given fin (for a given leg length) can be compactly represented when normalized as described above and shown in the figure. This is an interesting result, which implies that (for the motions studied here) the water environment, as seen by the hip joint, is accurately modeled as a strictly viscous environment (i.e., the torque load on each hip is proportional to the hip angular velocity).

3.2. Average torque, power, and thrust relationships of finned swimming

Figure 5 shows the span of frequencies and amplitudes of motion corresponding to each trial for both the long and short fins. Trials conducted with the long, stiff fins are indicated by circles, while trials conducted with the shorter, more flexible fins are indicated by crosses. Trials of similar amplitude across Figure 5 are indicated by similar color, with amplitude increasing with the darkness of the line color. Note that desired frequencies were reduced at increased amplitudes, due to torque and power limitations in the robotic swimmer (human swimmers would be similarly power-limited).

The joint power (shown in Figure 4(d)) was averaged over a stroke for each trial condition and plotted (in a non-amplitude-normalized form) against frequency in Figure 6(a), which also indicates amplitude by shade of color. Similarly, the measured thrust was also averaged across stroke and is shown plotted (non-normalized) against frequency in Figure 6(b), also with shade of color indicating motion amplitude.

The average mechanical power of a single hip joint for each trial is plotted against its measured thrust production in Figure 7. Note that thrust production in Figure 7 is presented as thrust per leg (i.e., the thrust production for a given trial is half its corresponding thrust production shown in Figure 6). Trials of like target motion amplitude are indicated by color. Though thrust and mechanical power are dependent on motion characteristics (i.e., amplitude and frequency), the relationship between thrust and mechanical power is essentially independent of motion amplitude.

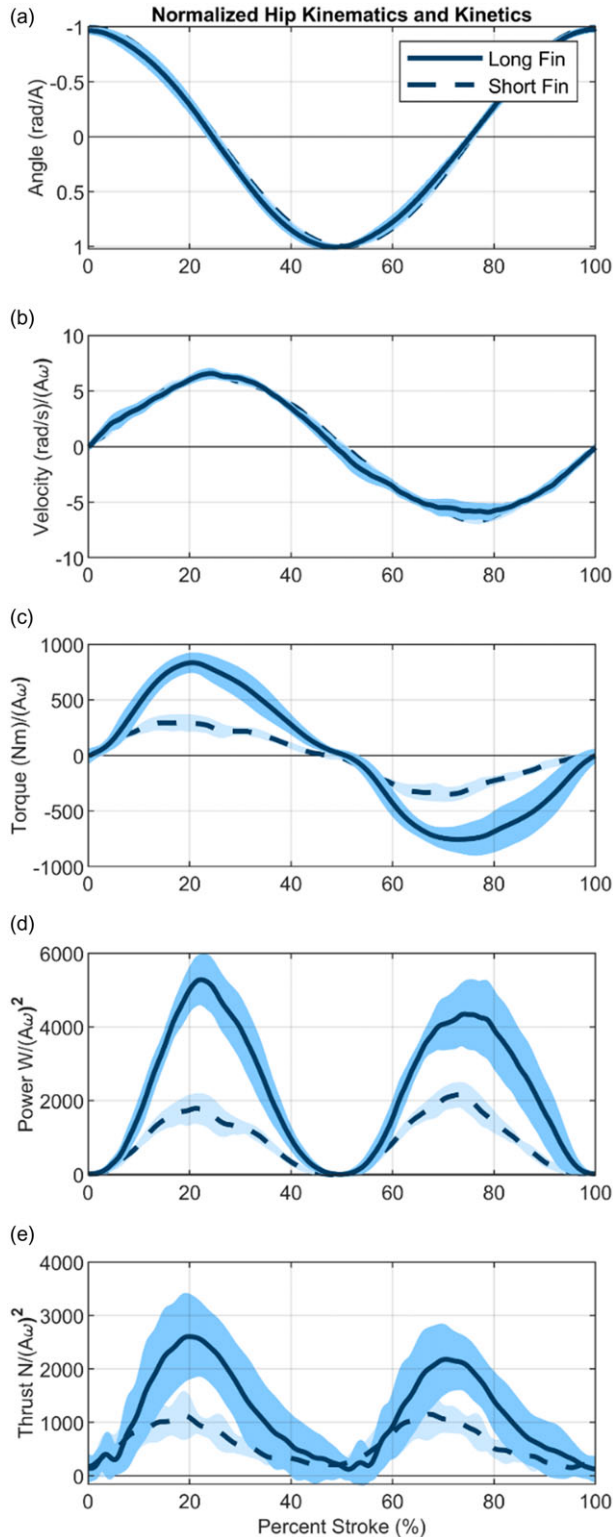


Figure 4. Time and amplitude-normalized kinematics and kinetics for the flutter kick motion with long, stiff fins (solid line) and short, flexible fins (dashed line). Note time normalization was done by division of frequency of motion (in Hz).

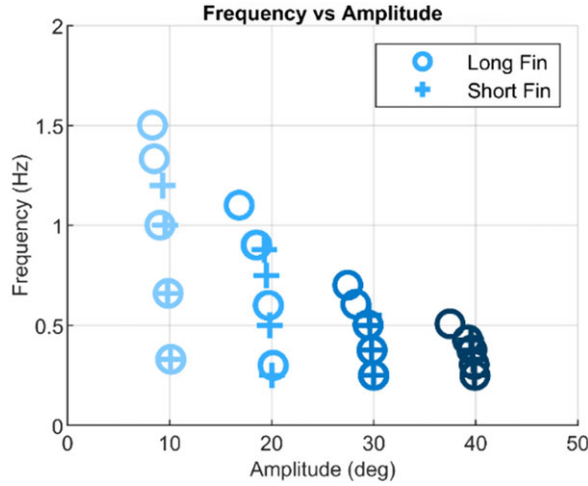


Figure 5. Stroke amplitudes and frequencies explored in experimental trials. Note amplitude refers to peak-to-peak amplitude.

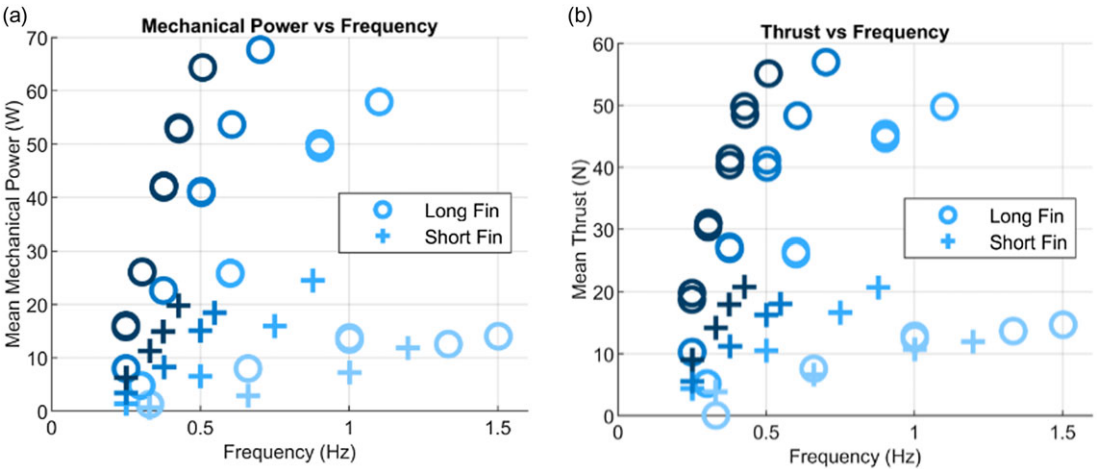


Figure 6. (a) Average mechanical power per joint (calculated from the measured velocity and torque at the hip joint) for each trial, and (b) Average thrust production measured for each trial.

3.3. Actuator requirements

To the extent that the amplitude-normalized dynamics and resulting thrust generation remain invariant across motion amplitudes and frequencies (as indicated by Figure 4), the data collected in the previously described trials can be used to project to higher levels of thrust, should a designer be interested in generating higher levels of thrust. Assuming the invariance holds, Figure 8 shows the projected mean joint torque and velocity corresponding to increased thrust production (Figures 8(a) and (b)), and also shows the mean torque and velocity associated with producing a given amplitude and frequency of motion for each fin type (Figures 8(c) and (d)). Note that, in this study, joint motion and torque were sinusoidal; thus, peak requirements can be calculated from the mean requirements (shown in Figure 8) accordingly.

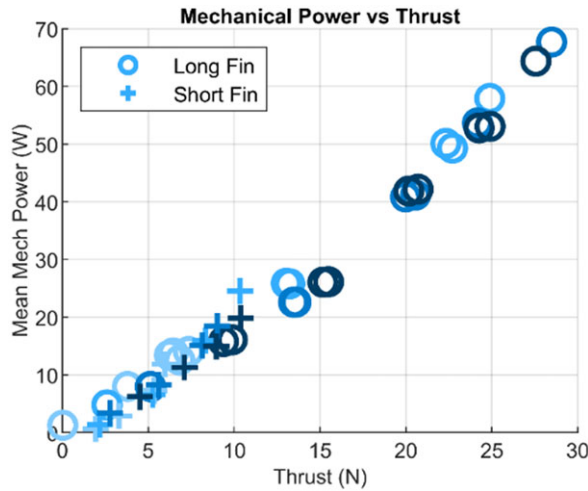


Figure 7. Measured mechanical power per hip of each trial plotted against the mean thrust generated per leg.

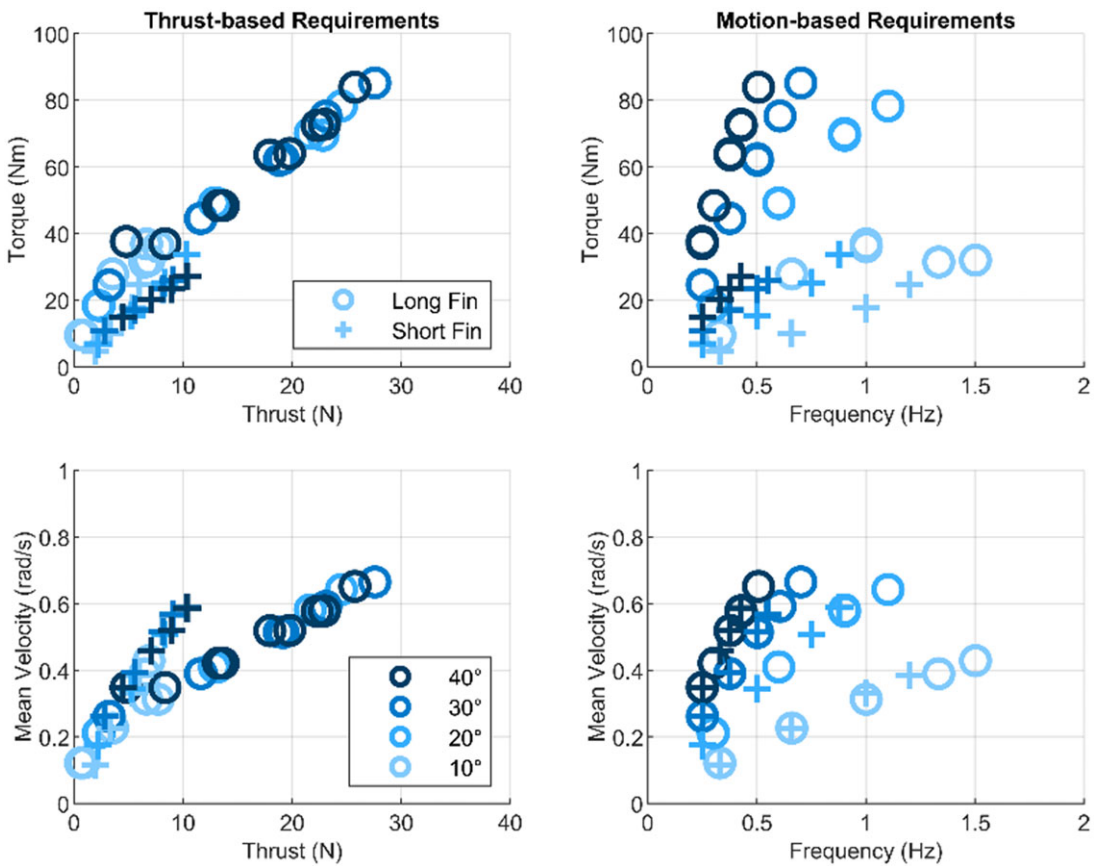


Figure 8. The mean torque (top) and speed (bottom) requirements to generate thrust (left) or motion characteristics (right), all given on a per-leg basis. Experimental data points are provided for operation with long, stiff fins (dashed line, circles) and short, flexible fins (dotted line, crosses). Motion-based projections were dependent on amplitude, indicated by the shade of plotted points.

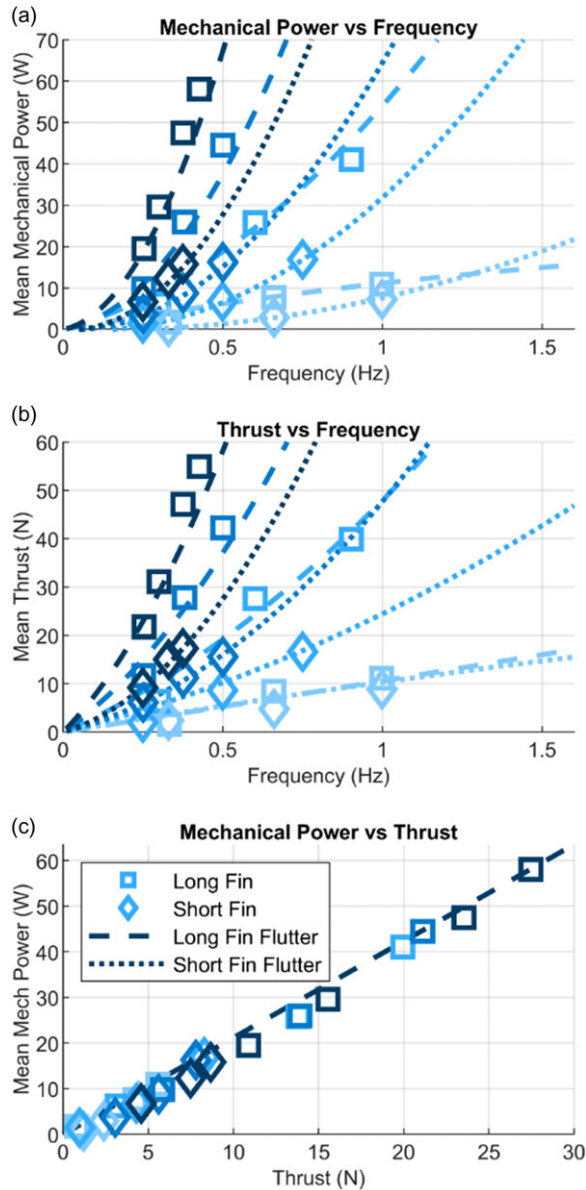


Figure 9. A comparison of the mechanical power and thrust requirements of the kicking with right and left legs in-phase versus out-of-phase.

3.4. Bilateral kicking in-phase

Experimental trials were repeated where the right and left hip motion were commanded to move in-phase, rather than 180 deg out-of-phase. Measured mechanical power and thrust are shown plotted against frequency of motion in Figure 9(a) and (b), respectively. Mechanical power for each trial is plotted against its corresponding thrust production in Figure 9(c). Squares indicate trials with the long, stiff fins, and a dashed line indicates a polynomial fit to corresponding data from the flutter kicking trials. Diamonds indicate trials with the short, flexible fins, and a dotted line indicates a fit to corresponding flutter kicking trials. Commanded motion amplitude is indicated by shade, with darker shades indicating larger motion amplitudes.

4. Discussion

4.1. Stroke-based kinematics and kinetics of finned swimming

Among the insights associated with this study is that joint-based motion, velocity, torque, and power of finned swimming, for a given fin, appear to be invariant when time and amplitude-normalized (time normalization by segmented stroke, amplitude normalization by motion amplitude for angle; product of motion amplitude and frequency for velocity and thrust; and square of product of motion amplitude and frequency for power), as shown in Figure 4. As such, one can reasonably well characterize joint-based torque and power requirements across all (sinusoidal) motions with a single sinusoidal motion (i.e., a trial at one amplitude and frequency can characterize joint kinetics at all amplitudes and frequencies), for a given set of fins. To the author's knowledge, this is the first presentation of this observation. Also, the same normalization applies to thrust generation, where thrust is also amplitude-normalized by the square of the product of motion amplitude and frequency (see Figure 4(e)). Therefore, for the range of motion amplitude and frequencies included in this study (i.e., 19 and 16 cases for each fin type, respectively), a single trial with a given fin and leg length could have reasonably characterized the joint requirements and resulting thrust across all motions for that fin and leg length.

An associated observation, based on the invariance of joint torque normalized by the product of motion amplitude and frequency, and also on the invariance of joint power normalized by the square of the product of motion amplitude and frequency, is that the aquatic environment acts as an approximate angular viscous resistance on the hip joint. This would have been a reasonable hypothesis without having performed experiments, but is not obvious given the complexities of fluid flow and fluid interaction with compliant members. As such, verification of the legitimacy of a viscous approximation is another notable observation of this work.

4.2. Relationship between kick amplitude, thrust, and power

As illustrated in Figure 6(b), a given amount of thrust can be produced with higher amplitude and lower frequency motion, or higher frequency and lower amplitude motion. As illustrated in Figure 7, the power-specific thrust (amount of thrust normalized by mechanical power at the hip joints) is invariant for a given fin type, across amplitudes and frequencies, at least for the span of amplitudes and frequencies measured here. However, since increasing amplitude of motion presumably increases the drag profile of the swimmer, it is possible that a lower amplitude, higher frequency movement might be preferable, at least without regard to the preference of a human swimmer. Since this study was conducted with a stationary swimmer, the increased drag associated with a greater kick amplitude was not accounted for. Additionally, though the lowest kick amplitude (10 deg) yielded thrust production commensurate with the mechanical power requirements, thrust did not increase as much as in trials of greater amplitude. Consider that a swim fin is a flexible member and deflects in response to drag forces imparted by the water. Once deflected, the fin allows for effective transmission of mechanical power to the water. However, a 10 deg amplitude, particularly for the long fin, did not seem sufficient to fully leverage the fin deflection to impart substantial amounts of mechanical work to the water and therefore did not seem capable of producing thrust comparable to greater amplitudes of motion. Thus, thrust production does not seem to depend on kick amplitude insofar as the kick is sufficiently large enough to achieve a given minimum fin deflection. Therefore, the lower bound on a desired amplitude relates to achieving sufficient fin deflection, while an upper limit might be related to limiting drag forces due to an increased frontal profile in the water.

4.3. Effect of fin type

Two fins were utilized in this study: (1) a long, stiff fin and (2) a short, flexible fin. Trials with the long stiff fin yielded the greatest thrust production. However, both fins displayed a similar power-specific thrust. For a given thrust level, fin type primarily influences the relationship between torque and velocity.

Specifically, the long, stiff fin generated thrust while moving at a lower speed than the short, flexible fin, but while requiring greater torque. The increased torque requirement was most notable at low levels of mechanical power. As mechanical power and thrust production were increased, the difference in the torque-specific thrust production of each of the fins decreased, but the shorter fins required significantly higher motion velocities to generate thrust commensurate with the longer fins.

4.4. “Ideal” kicking and efficient thrust production

A preferred kicking motion for purposes of thrust generation, as discussed in ref. [17], is executed with a fully extended knee and ankle, effectively forming a rigid connection between the fin and hip and transiently coordinating their motions. A robotic swimmer can leverage passive supports to facilitate an ideal kicking motion. Such motion is achieved in humans by isometric contraction of the leg muscles to hold the knee and ankle extended and couple the motion of the fin and the hip. During the power stroke, the torque generated by the fin about the ankle joint aids extension, but the knee must be held extended throughout the motion. This reverses during the recovery stroke – the ankle must be held extended while the drag produced by fin motion aids in knee extension. The joints struggle to maintain their position as they slow and as the direction of the torque they must oppose changes, compromising the extension of the knee and ankle. This compliance not only reduces the magnitude of thrust generated throughout the stroke, but often results in negative thrust production, and also delays the start of the next stroke, further reducing the possible thrust production of the movement. While the thrust production of the swimming stroke is decreased, compliance at the knee and ankle reduces the torque and power requirements of the hip, which may alternatively be the limiting factor in a swimmer’s ability to execute an ideal stroke depending on muscular strength, endurance, and fitness. Thus, relationships between mechanical power, thrust production, and stroke kinematics may differ for a robotic swimmer compared to a human swimmer.

In this work, rigid supports were used to connect the actuated hip joint to the swim fin. Some level of compliance between the hip and fin could be beneficial to thrust production, but the thrust production measured in this study suggests that this rigid coupling is preferable to a human’s ability to coordinate the hip and fin. Specifically, prior works measuring the kinematics and thrust production of human finned swimming report kick amplitudes of roughly 20 to 40 deg, kick frequencies ranging from approximately 0.5 to 1.5 Hz, and average thrust production of approximately 10 to 50 N [13–15, 18]. In comparison, the robotic swimmer achieved 50 N of thrust with kick frequencies of 0.5, 0.7, and 1.1 Hz at amplitudes of 40, 30, and 20 deg, respectively. Additionally, in human swimming, instances of negative thrust are frequently observed, often during reversal periods. Though the thrust production of the robotic swimmer was decreased during transition periods, the device produced comparably little negative thrust during the stroke, and many trials did not yield any instances of negative thrust.

4.5. Actuator requirements

The experimental data collected in this study may serve as a reference to inform the design of future robotic swimmers. Torque and speed requirements as a function of desired thrust production and desired motion are shown in Fig 8. The plots on the left side of Figure 8 provide torque and speed requirements for a desired level of thrust production. Recall that the torque signature and the fin motion were approximately sinusoidal. As such, the torque requirement corresponds roughly to the mean of a sin wave utilized to drive hip motion, and the mean velocity requirement corresponds to the mean velocity of sinusoidal motion. Peak requirements can be calculated accordingly, and note that the peak torque and velocity are aligned transiently, and thus the actuator must deliver peak torque at peak speed. The plots on the right side of Figure 8 show torque-speed requirements for desired motion characteristics, presented in terms of kick amplitude and frequency. Thus, if designing for thrust production, the left plots of Figure 8 may be utilized, and if designing for desired motion, the right plots may be utilized as a reference for required actuator characteristics. If the left is used, the right can be used to approximate

the motion characteristics corresponding to the desired thrust production, and if the right is used, the left can be used to approximate the thrust production of the desired motion.

The projections presented in this work are intended to suggest the potential capabilities of a robotic swimmer, whether intended to operate as a standalone unit or for use in collaboration with a human swimmer. Further, the projections are intended to inform the design of such a device by projecting the torque and speed requirements of actuation based on the desired thrust or motion characteristics. If intended to function as a standalone unit or for an assistive application, all power and torque must necessarily be provided by an actuator, but if used collaboratively with a human, the device need not provide all torque required for a given motion, as the human would be expected to contribute some portion.

4.6. *Kicking in-phase versus out-of-phase*

The effect of moving the right and left hips out-of-phase relative to moving them in-phase is summarized in Figure 9. As can be seen in these plots, the two cases show very little if any differences (i.e., the differences are not discernable relative to the variance in the data). As such, the phasing between right and left legs appears to have little effect on the relationship between hip joint motion (and torque and power) and thrust generation.

Although the phasing of kicking motion does not appear to be a significant factor in thrust production, one should consider some issues related to this observation. With reference to the torque requirements for each hip joint shown in Figure 4(b), phasing the two hip joints 180 deg out-of-phase will better balance the torques in the hip structure, thus minimizing the external torques between the robot and environment (or between the robot and human, in the case that the robot is an exoskeleton).

5. Conclusion

This paper presents an experimental investigation that maps the torque and power requirements associated with human finned swimming to the resultant underwater thrust generation. The data is intended to inform the development of a lower limb exoskeleton to augment finned swimming. Experiments were conducted on a robotic testbed to characterize the hip torque and power required at various amplitudes and frequencies of hip motion to generate underwater thrust. Among the significant observations to inform the design of a robotic lower limb exoskeleton: (1) the underwater environment can be accurately modeled as a simple viscous load as seen by the hip joints, where viscous coefficient depends on the type of fin; (2) accordingly, for a given fin, movement at any amplitude and frequency is invariant when motion is normalized by amplitude; velocity and torque by the product of amplitude and frequency; and power and thrust by the square of the product of amplitude and frequency; (3) the power-specific thrust is invariant, regardless of fin type, amplitude of motion, and frequency of motion; and (4) the phasing between right and left legs does not have a significant effect on thrust generation (i.e., flutter and dolphin kick behave similarly).

Supplementary material. The supplementary material for this article can be found at <https://doi.org/10.1017/S0263574724001231>.

Author contributions. BJ designed the experimental apparatus and controller described in the paper. He conducted the experimental trials and processed all data. MG advised and oversaw the process, giving feedback throughout.

Financial support. This work was supported by the National Science Foundation Graduate Research Fellowship Award number 259174

Competing interests. The authors declare no conflicts of interest exist.

Ethical approval. None.

References

- [1] A. J. Young and D. P. Ferris, “State of the art and future directions for lower limb robotic exoskeletons,” *IEEE Trans Neur Syst Rehabil Eng* **25**(2), 171–182 (2017).
- [2] D. A. Winter, Biomechanics and motor control of human gait: Normal elderly and pathological, (1991).
- [3] J. Camargo, A. Ramanathan, W. Flanagan and A. Young, “A comprehensive, open-source dataset of lower limb biomechanics in multiple conditions of stairs, ramps, and level-ground ambulation and transitions,” *J Biomech* **119**, 110320 (2021).
- [4] Y. Zhong, Z. Li and R. Du, “A novel robot fish with wire-driven active body and compliant tail,” *IEEE/ASME Trans Mechatr* **22**(4), 1633–1643 (2017).
- [5] F. Lyu, X. Xu, X. Zha, Z. Li and H. Yuan, “A Snake Eel Inspired Multi-joint Underwater Inspection Robot for Undersea Infrastructure Intelligent Maintenance,” *In: OCEANS 2022*, (2022) pp. 1–6.
- [6] Z. Shen, J. Na and Z. Wang, “A biomimetic underwater soft robot inspired by cephalopod mollusc,” *IEEE Robot Autom Lett* **2**(4), 2217–2223 (2017).
- [7] G. Chen, Y. Xu, Z. Wang, J. Tu, H. Hu, C. Chen, Y. Xu, X. Chai, J. Zhang and J. Shi, “Dynamic tail modeling and motion analysis of a beaver-like robot,” *Nonlinear Dynam* **112**(9), 6859–6875 (2024).
- [8] M. Nakashima, T. Koga and H. Takagi, “Measurement of Propulsive Forces in Swimming by Using a Swimming Humanoid Robot,” *In: 21st International Conference on Control, Automation and Systems (ICCAS)*, (2021) pp. 1780–1783.
- [9] Y. Li, E. Shimizu and M. Ito, “Development of a humanoid robot for underwater use,” *Artif Life Robot* **15**(4), 551–554 (2010).
- [10] Q. Wang, Z. Zhou, Z. Zhang, Y. Lou, Y. Zhou, S. Zhang, W. Chen, C. Mao, Z. Wang, W. Lou and J. Mai, “An underwater lower-extremity soft exoskeleton for breaststroke assistance,” *IEEE Trans Med Robot Bio* **2**(3), 447–462 (2020).
- [11] P. D. Neuhaus, M. O. O’Sullivan, D. Eaton, J. Carff and J. E. Pratt, “Concept Designs for Underwater Swimming Exoskeletons,” *In: IEEE International Conference on Robotics and Automation, 2004. Proceedings. ICRA ’04*, (2004) pp. 4893–4898.
- [12] H. Xia, M. A. Khan, Z. Li and M. C. Zhou, “Wearable robots for human underwater movement ability enhancement: A survey,” *IEEE/CAA J Autom Sin* **9**(6), 967–977 (2022).
- [13] D. R. Pendergast, J. Mollendorf, C. Logue and S. Samimy, “Evaluation of fins used in underwater swimming,” *J Undersea Hyperb Med Soc* **30**(1), 57–73 (2003).
- [14] S. Samimy, J. C. Mollendorf and D. R. Pendergast, “A theoretical and experimental analysis of diver technique in underwater fin swimming,” *Sports Eng* **8**(1), 27–38 (2005).
- [15] P. Zamparo, D. R. Pendergast, B. Termin and A. E. Minetti, “How fins affect the economy and efficiency of human swimming,” *J Exp Biol* **205**(17), 2665–2676 (2002).
- [16] B. P. Johnson and M. Goldfarb, “Towards a Finned-Swimming Exoskeleton: A Robotic Flutter Kicking Testbed and its Corresponding Thrust Generation,” *In: 2023 IEEE International Conference on Robotics and Automation (ICRA)*, (2023) pp. 10471–10477.
- [17] M. Wojtków and A. Nikodem, “Biomechanics of diving: The influence of the swimming speed on the kinematics of lower limbs of professional divers,” *Acta Bioeng Biomech* **19**(4), 117–125 (2017).
- [18] R. A. Christianson, G. Weltman and G. H. Egstrom, “Thrust forces in underwater swimming,” *Hum Factors* **7**(6), 561–568 (1965).

Cite this article: B. Johnson and M. Goldfarb, “Torque, speed, and power requirements for the design of a lower limb exoskeleton to augment human finned swimming”, *Robotica*. <https://doi.org/10.1017/S0263574724001231>